

Distribution Agreement

In presenting this thesis as a partial fulfillment of the requirements for a degree from Emory University, I hereby grant to Emory University and its agents the non-exclusive license to archive, make accessible, and display my thesis in whole or in part in all forms of media, now or hereafter now, including display on the World Wide Web. I understand that I may select some access restrictions as part of the online submission of this thesis. I retain all ownership rights to the copyright of the thesis. I also retain the right to use in future works (such as articles or books) all or part of this thesis.

Sarah Abraham

April 10, 2023

Investigation of an Improved Phospholipid-Mimicking Agonist of LRH-1

By

Sarah Abraham

Eric Ortlund

Adviser

Biology

Eric Ortlund

Adviser

Jitendra Thakur

Committee Member

Brian Dyer

Committee Member

2023

Investigation of an Improved Phospholipid-Mimicking Agonist of LRH-1

By

Sarah Abraham

Eric Ortlund

Adviser

An abstract of
a thesis submitted to the Faculty of Emory College of Arts and Sciences
of Emory University in partial fulfillment
of the requirements of the degree of
Bachelor of Science with Honors

Biology

2023

Abstract
Investigation of an Improved Phospholipid-Mimicking Agonist of LRH-1

By Sarah Abraham

Liver receptor homolog-1 (LRH-1; NR5A2) is a nuclear receptor that regulates glucose and bile acid homeostasis in the liver, intestine, and pancreas. We have recently reported small molecules that mimic phospholipid residue contacts at the binding pocket mouth through carboxylic acid tails. Here, we report a similar series of small molecules with different polar moieties that aim to make similar contacts. Using a tetrazole instead of the carboxylic acid improves potency, target gene expression, and binding at the mouth of the pocket. Combining a previous small molecule with the tetrazole design improves compound potency, binding, and thermal stability. The resulting small molecule is specific for NR5A receptors providing a useful tool for exploring LRH-1 biology and targeting the receptor in pathophysiological contexts.

Investigation of an Improved Phospholipid-Mimicking Agonist of LRH-1

By

Sarah Abraham

Eric Ortlund

Adviser

A thesis submitted to the Faculty of Emory College of Arts and Sciences
of Emory University in partial fulfillment
of the requirements of the degree of
Bachelor of Science with Honors

Biology

2023

Acknowledgments

My thanks to my adviser, Dr. Eric Ortlund and Dr. Michael Cato for their support and help over the past two years. I would also like to thank my other committee members Jitendra Thakur and Brian Dyer as well.

Table of Contents

Introduction.....	1
Results.....	4
Discussion.....	12
Methods.....	15
References.....	24
Supplemental Information.....	28

Introduction:

Inflammatory Bowel Disease (IBD) is a class of diseases characterized by chronic inflammation of the gastrointestinal tract and affects approximately 3.1 million people in the US (Xu et al., 2018). Glucocorticoids (GCs) are a common treatment for IBD. While GCs reduce gut inflammation, they also may have unwanted side effects that result from tissues outside the intestines necessitating the need for new therapies that promote local glucocorticoid synthesis (Al-Barwardy et al., 2021; Bayrer et al., 2018; Bruscoli et al., 2021).

Nuclear receptors (NRs) are a class of transcription factors that modulate gene expression in response to lipophilic molecules. Most NRs consist of a DNA binding domain (DBD), ligand binding domain (LBD), and hinge region. Ligand binding induces conformational changes within the NR that drive coregulator association, which remodel chromatin and recruit transcriptional machinery (Evans and Mangelsdorf, 2014; Li et al., 2003; Lonard and O'Malley B, 2007; McKenna et al., 1999; Nagy and Schwabe, 2004; Weikum et al., 2018). Liver receptor homolog -1 (LRH-1; NR5A2) is a member of the NR5A subclass of NRs and is primarily expressed in tissues such as the breast, ovaries, and tissues of endodermal origin, such as the pancreas, intestines, and the liver. LRH-1 has regulatory roles in glucose and bile acid homeostasis, steroidogenesis, and development (Stein and Schoonjans, 2015; Yazawa et al., 2015). LRH-1 is also involved in cell renewal and glucocorticoid synthesis within epithelial cells in the gut, making it an attractive target for IBD (Botrugno et al., 2004; Coste et al., 2007; Fernandez-Marcos et al., 2011; Mueller et al., 2006).

While the endogenous ligand for LRH-1 remains disputed, crystal structures and mass spectrometry have shown that LRH-1 binds phospholipids (PLs) (Sablin and Krylova et al., 2005; Ortlund et al., 2005). Phosphatidylcholines of medium tail length are the most activating and

drive coactivator recruitment *in vitro* (Musille et al., 2012). Additionally, dilauroylphosphatidylcholine (DLPC), a dietary phospholipid, decreased glucose intolerance and liver steatosis, while downregulating genes involved in lipogenesis in a murine high-fat diet model (Lee et al., 2011). However, PL's are a poor tool for clinical and laboratory use due to their insolubility and poor potency, making synthetic agonists a much more attractive tool for modulating LRH-1 activity.

The first class of LRH-1 agonists bound deep within the pocket in a manner dissimilar to that of phospholipids (**Fig. 1A, B**). RJW100, the lead molecule of this class, contacted deep polar residues through waters that are conserved within the binding pocket (**Fig. 1B, C**) (Mays et al., 2016; Whitby et al., 2006; Whitby et al., 2011). To mimic interactions that phospholipids make with the pocket mouth, compounds with various carbon chain lengths and phospho-mimetic moieties were synthesized. 10CA emerged as the lead compound of this investigation and included a carboxylic acid at the end of a ten-carbon linker (**Fig. 1B, C**). This compound displayed improved potency and efficacy relative to RJW100 in reporter assays (Flynn et al., 2018). Later structural studies confirmed that 10CA contacts the same polar residues as phospholipids at the pocket mouth (G421, Y516, and K520) (**Fig. 1B**) (Mays et al., 2022).

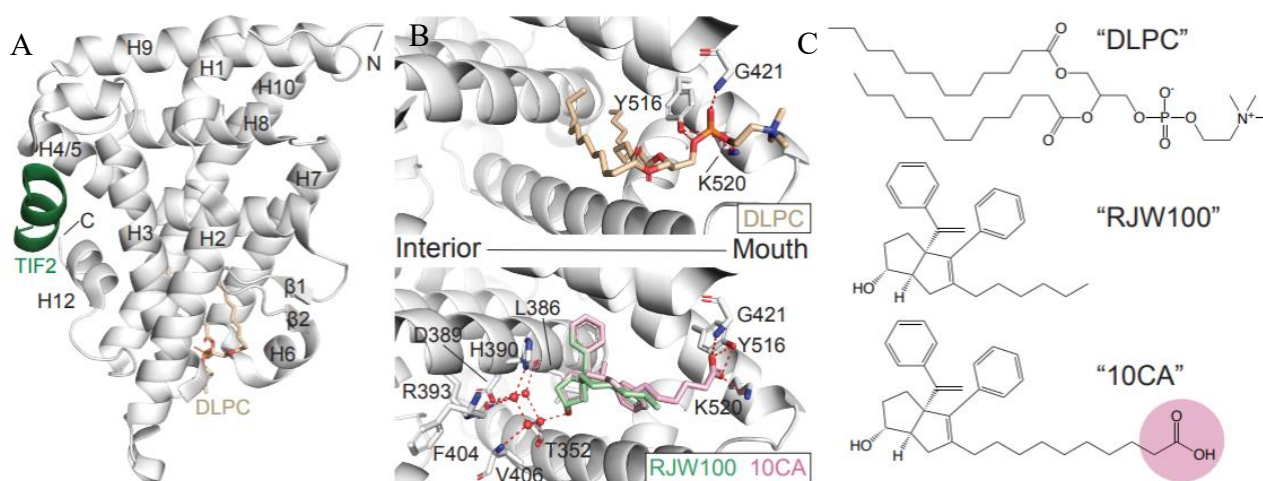


Figure 1. LRH-1 binding to agonistic ligands. **A.** Structure of LRH-1 (light grey; PDB entry 4DOS) bound to DLPC (beige) and TIF2 coactivator peptide fragment (green). **B.** Binding orientation of DLPC within the pocket mouth (top; beige; PDB 4DOS) and RJW100 (bottom; green; PDB entry 5L11) overlaid with phospholipid-mimetic small molecule 10CA (bottom; light pink; PDB entry 7JYD). Interacting side chains are shown as sticks (O = red, N = blue, P = orange, C = white). Hydrogen bonds are indicated with red dotted lines and waters necessary for small molecule-LRH-1 interactions are shown as red spheres. **C.** Chemical structures of DLPC, RJW100, and 10CA.

Previously, various polar moieties on the core of the RJW100 have been explored that sought to make direct contact with polar residues indirectly engaged through the conserved water network (**Fig. 1B**). The lead compound from these studies ('6N') replaced the hydroxyl group with a sulfamide, which improved binding affinity and agonism (D'Agostino et al., 2020). However, few alternative functional groups to the carboxylic acid have been explored. Therefore, we developed a series of 10CA isosteres to investigate the effects of different pocket mouth contacts (Allen et al., 2012; Friedman, 1951; Wassermann and Bajorath, 2011).

Replacing the carboxylic acid with a tetrazole moiety improved potency and increased target gene expression in HepG2 cells. Investigation of the tetrazole through structural studies paired with molecular dynamics (MD) revealed that the tetrazole preserved allosteric communication similar to that of 10CA and improved hydrogen binding at the pocket mouth. Adding the 6N sulfamide to the tetrazole isostere improves binding and potency further. The resulting small molecules ('6N-Tet') showed specificity for NR5A receptors, providing a useful tool for LRH-1 activation both within laboratory and clinical settings.

RESULTS:

10CA isosteres were designed with a variety of polar moieties, including a tetrazole ('Tet'), amide ('Am'), hydroxamic acid ('HA'), piperazine ('PIP'), sulfamate ('Sul'), and serine ('Ser') (Fig. 2).

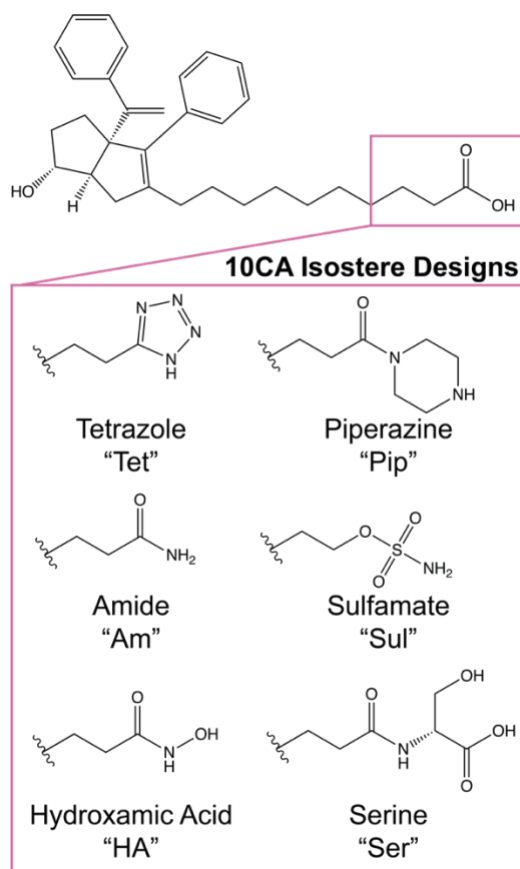


Figure 2. Chemical structures of 10CA isostere series.

To begin the investigation, we tested compound binding to the LRH-1 LBD, using a fluorescence polarization competition assay (D'Agostino et al., 2020). The tetrazole had the highest binding affinity ($K_i = 23$ nM), similar to that of 10CA ($K_i = 26$ nM) (Fig. 3A, Supp Fig. 1A, B). The tetrazole also drove the greatest improvement of LRH-1 LBD stability and was the most congruent to 10CA (+6.4 °C and +6.65 °C, respectively) (Fig. 3B). We then assessed LRH-

1 activity using a luciferase reporter assay. Both the Tet ($EC_{50} = 710$ nM) and the Sul ($EC_{50} = 470$ nM) had improved potency relative to 10CA (**Fig. 3C, Supp. Fig. 2**). The other isosteres displayed either decreased potency, thermal stability and/or affinity. To further investigate the effects of the compounds on LRH-1 activity, we tested the effect of compounds on the expression of two target genes of LRH-1 in liver-derived HepG2, cells which are commonly used for examining LRH-1 activity (Cato et al., 2022; Choi et al., 2020; Whitby et al., 2006; Xiao et al., 2018). Genes examined included *CYP7A1*, which encodes the rate limiting enzyme in bile acid homeostasis and *NR0B2*, which encodes a key nuclear receptor coregulator of LRH-1 (Li et al., 2005; Song et al., 2008). Tet drove the greatest increase in steady-state mRNA levels for both target genes (**Fig. 3D**). Therefore, Tet displays improved potency and efficacy over 10CA and was thus used for future mechanistic exploration.

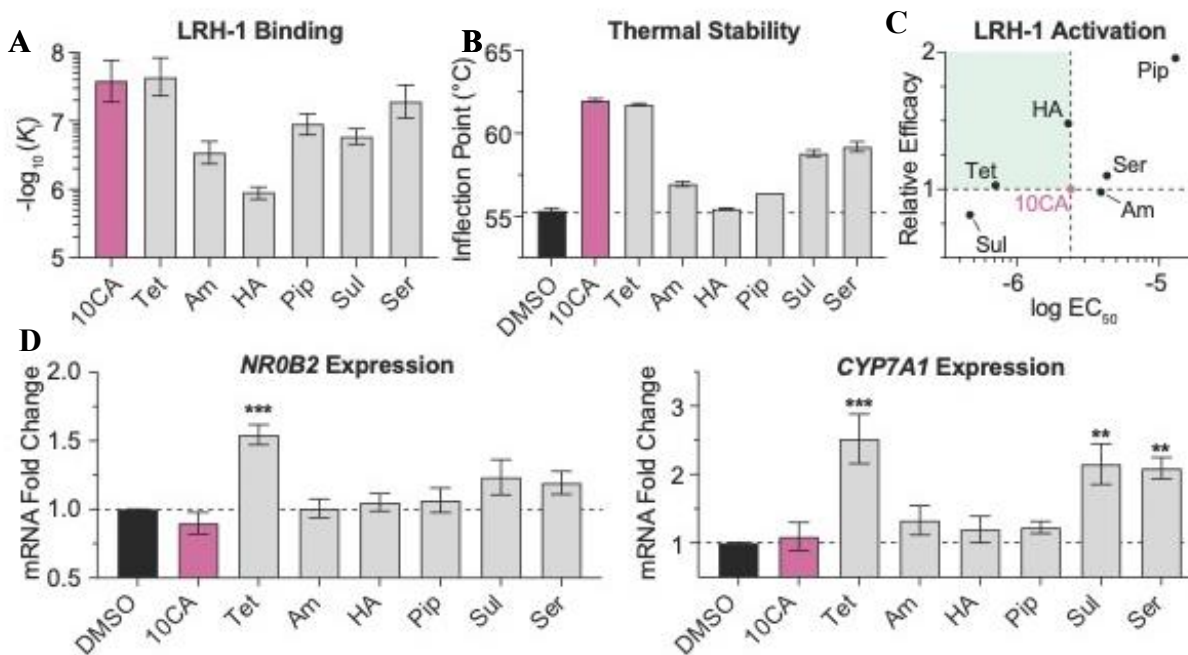


Figure 3. Biochemical characterization of 10CA isostere series. A. FP competition assay assessing binding affinity of compounds for the LRH-1 LBD. K_i = inhibition constant. Data from two independent experiments are

shown as means \pm 95% confidence intervals. **B.** Ligand-driven thermal stability of LRH-1 LBD. The inflection point corresponds to the temperature at which the protein unfolds. Data from two independent experiments are shown as means \pm SEM. **C.** Luciferase reporter assay used to determine compound-mediated activation of LRH-1. Relative efficacy was calculated by normalization the fold change to that of 10CA. The green quadrant indicates increased potency and efficacy relative to 10CA. Data is shown as a means from three biological replicates. **D.** RT-qPCR analysis of HepG2 cells treated with isosteres (Tet and Sul – 10 μ M; 10CA, Am, HA, Pip, and Ser – 30 μ M) for 24 hours. Data from four biological replicates were normalized to DMSO control and are shown as means \pm SEM. Brown-Forsythe and Welch one-way ANOVA with Dunnett multiple comparison test, ** $p < 0.01$, *** $p < 0.001$.

To investigate the mechanism of Tet, we solved the crystal structure of the LRH-1 LBD bound to Tet and a fragment of a common NR coactivator TIF2. There was electron density that corresponds to the tail, core, and tetrazole group (**Fig. 4A,B; Table S1**). The tetrazole position was very similar to that of the carboxylic acid of 10CA (**Fig. 4C**). Tet and 10CA both make the same deep polar contacts via the conserved water network (**Fig. 4C**) (Mays et al., 2022; Mays et al., 2016). Although the tetrazole had more extensive contacts at the mouth of the pocket, there was no contact with K520 (**Fig. 4D**). This may be due to the low pH (4.6) of crystallization conditions, potentially protonating the tetrazole and consequently decreasing the electrostatic interaction with the nearby lysine.

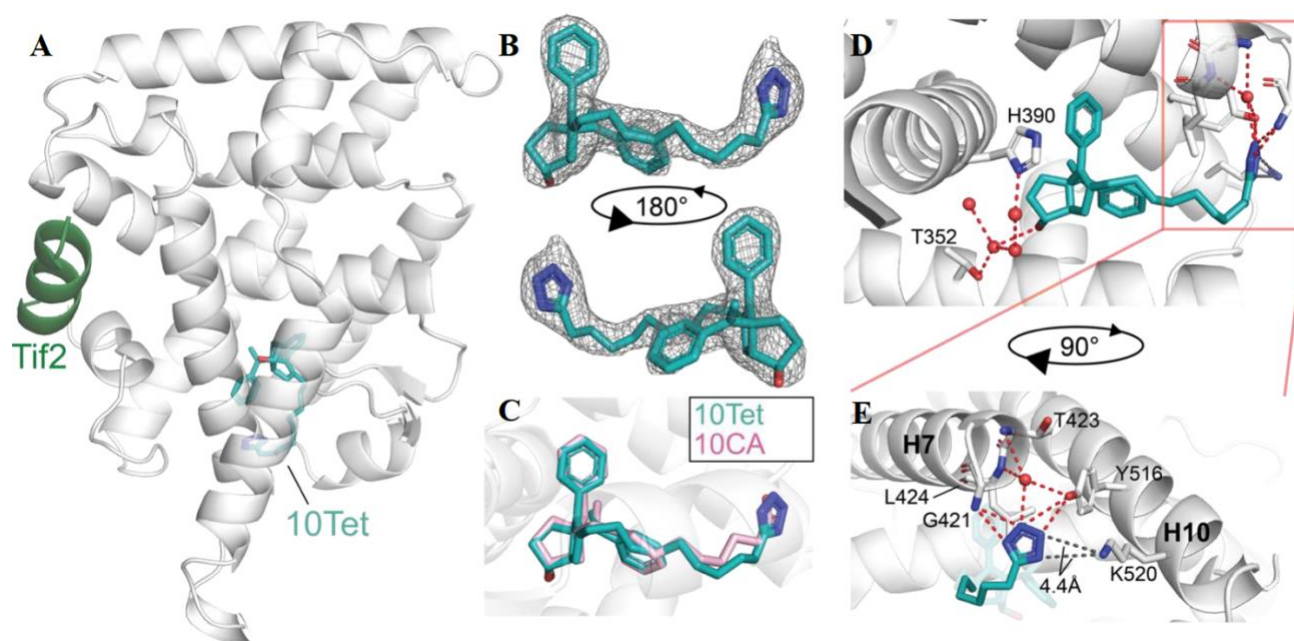


Figure 4. Crystal structure of LRH-1 LBD with Tet and TIF2. **A.** Crystal structure of Tet (blue) bound to LRH-1 LBD (white; unpublished), and TIF2 peptide (green). **B.** Ligand $2F_o - F_c$ omit map showing electron density for Tet contoured at 1σ . **C.** Tet (blue) and 10CA (pink; PDB entry 7JYD) overlaid within the pocket. **D.** Deep pocket hydrogen bonding between Tet, water molecules (red spheres), and nearby residues. **E.** Tet interactions with pocket mouth residues. Sidechains (or mainchains) of interacting residues are shown as sticks (O = red, N = blue, S = yellow, C = white). Hydrogen bonds shown as red dotted lines. K520 is out of hydrogen bonding range (indicated by gray dotted lines).

Given the differences in interaction with K520 between Tet and 10CA we wanted to look at pocket mouth interactions. To do this, we used molecular dynamics (MD) for 4 * 500 ns simulations to determine which residues the ligands were interacting with. We looked at both the deprotonated tetrazole and the deprotonated carboxylic acid states, as they reflect ligand status at the physiological pH (Herbst and Wilson, 2002; Herr, 2002; Kaczmarek et al., 1979; Liljebris et al., 2002; Matta et al., 2010; McManus and Herbst, 2002; Neochoritis et al., 2019). Tet made stronger contact with the pocket mouth residues by interacting with specific residues for a larger

portion of the simulation time. The tetrazole moiety interacted with G421 for twenty times longer than 10CA and Y516 and K520 for two times as long (**Fig. 5A**). Upon comparison of the average structure, both 10CA and Tet mobilized H6-H7 (**Fig. 5B**). H6-H7 is where the alternative activation function surface (AF-B) is located which communicates ligand binding status to coregulators in LRH-1. (Musille et al., 2016; Musille et al., 2012).

Then, we performed a community analysis, which looks at groups of residues that have correlated motion to examine differences in communication between the ligand binding pocket and the AF-B. This analysis also allows for comparison between the apo state and the ligand-bound state (Girvan and Newman, 2002; Sethi et al., 2009; Vanwart et al., 2012). Of note, both 10CA and Tet drive correlated motion between the ligand binding pocket and H6-H7, which suggests that both ligands drive correlated motion to the AF-B (**Fig. 5C**). Another notable difference is that the correlated motion of the TIF2 peptide differed from the Tet- and 10CA-bound LBD, which suggests that different ligands may have altering effects on coactivator communication in certain contexts (**Fig. 5C**). Overall, the MD simulations predict that Tet makes stronger contacts at the pocket mouth and drives allosteric communication at the AF-B in a 10CA-like manner.

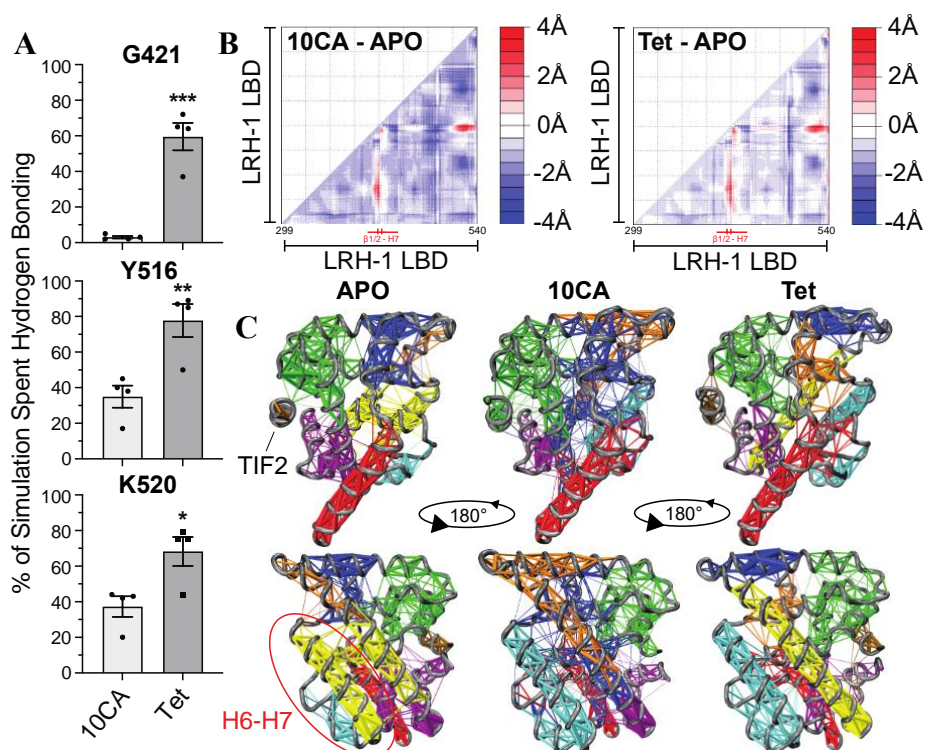


Figure 5. A. Duration of simulation Tet and 10CA spend hydrogen bonding with G421, Y516, and K520. Data is shown as means from four 500 ns simulations \pm SEM. Data was analyzed with an unpaired two-tailed t-test, * $p < 0.05$, ** $p < 0.01$, *** $p < 0.001$. **B.** Differences in average structures obtained by subtracting distances between residues and distance matrices (between C α atoms). Matrices are representative of structural changes between the two indicated complexes. **C.** Analysis showing communities of residues with high correlated motion. Edge weight is determined by degree of correlated motion.

Previously, replacing of the hydroxyl group on the RJW100 core with a sulfamide improved agonism and affinity ('6N') (Mays et al., 2019). Recently, we have found that a 'hybrid' of the two lead agonists ('6N-10CA') (Cato et al., 2022), demonstrated improved compound binding while maintaining high efficacy. Following similar logic, we appended the sulfamide to Tet, which improved binding, potency, and thermal stability (Fig. 6B, C, D, E). Additionally, 6N-Tet promoted similar levels of *NR0B2* mRNA to that of Tet (Fig. 6F).

Therefore, the addition of the sulfamide improves compound binding while upholding agonistic function that is modulated by pocket.

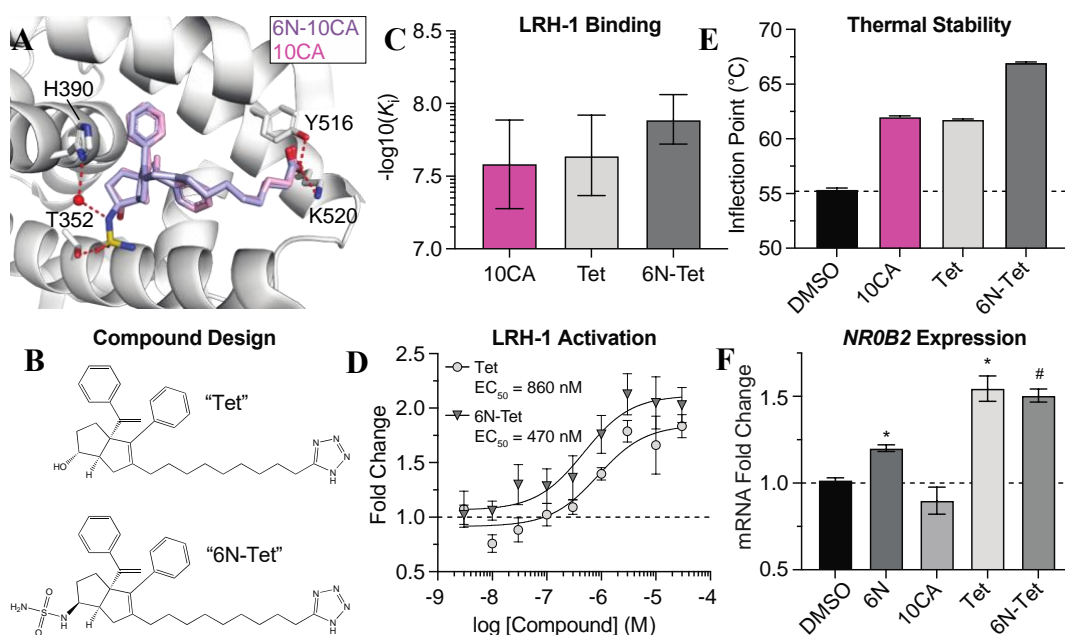


Figure 6. Characterization of 6N-Tet. **A.** Overlaid structure of 6N-10CA (purple; PDB entry 7TT8) and 10CA (pink; PDB entry 7JYD) in the LRH-1 LBD binding pocket. Residues that interact with ligands are shown in sticks (O = red, N = blue, S = yellow, C = white). Water molecules are shown as red spheres, and hydrogen bonds are shown in red dotted lines. **B.** Chemical structures of Tet and 6N-Tet. **C.** FP competition assay measuring the binding of compounds to the LRH-1 LBD. K_i = inhibition constant. Data from two independent experiments are shown as means \pm 95% confidence intervals. **D.** Luciferase reporter assay measuring compound-mediate activation of LRH-1. EC_{50} = maximal effective concentration. Data shown as means from three (Tet) or five (6N-Tet) biological replicates. **E.** Ligand-driven thermal stability of LRH-1 LBD. The inflection point corresponds to the melting temperature of the protein. Data from two independent experiments are shown as means \pm SEM. **F.** RT-qPCR analysis of HepG2 cells treated with agonists (Tet, 6N-Tet – 10 μ M; 10CA – 30 μ M) for 24 hours. Data from two (DMSO and 6N-Tet) or four (10CA and Tet) biological replicates. Data normalized to signal of DMSO control and shown as means \pm SEM.

The only other human NR5A receptor is steroidogenic factor-1 (SF-1, NR5A1) which shares ~76% sequence similarity in its LBD with that of LRH-1 (Sablin et al., 2003). All small molecules tested were cross-reactive with SF-1 (**Fig. 7A**). However, aside from the slight activation of PXR, 6N-Tet showed no activation for other NRs tested, such as ER α , AR, and GR (**Fig. 7B**). Overall, the Tet isostere improves compound potency and LRH-1 target gene expression while also maintaining high affinity for LRH-1 and specificity for NR5A receptors.

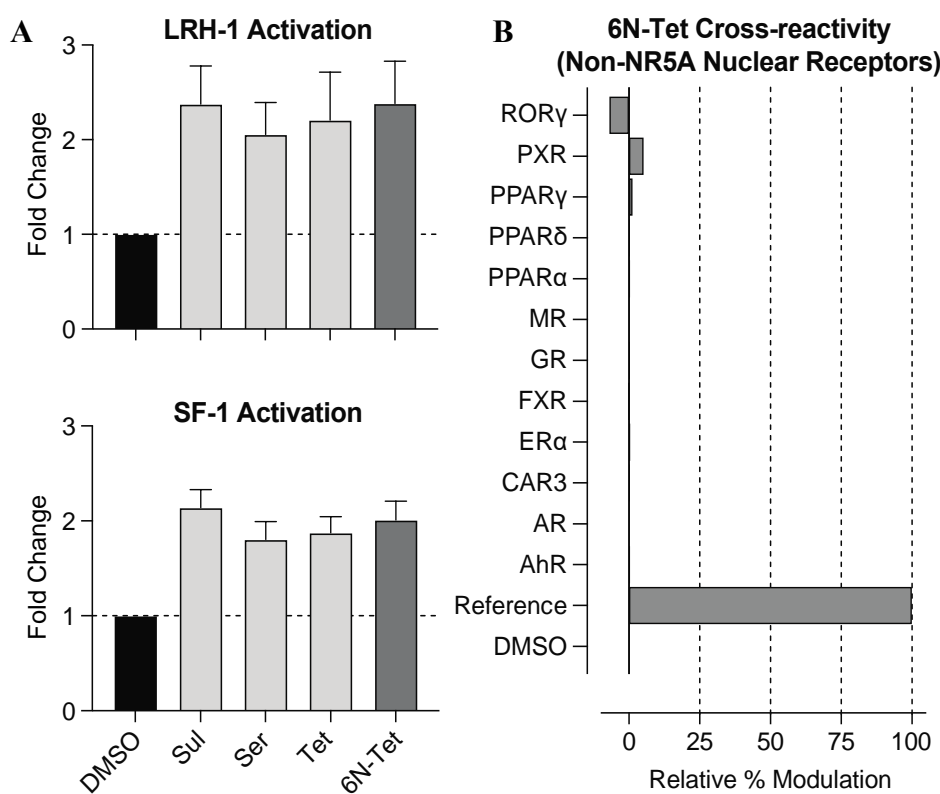


Figure 7. Cross reactivity studies for LRH-1 small molecules. **A.** Luciferase reporter assay showing activation of LRH-1 and SF-1 with 10 μ M of indicated compounds. Data from four biological replicates represented as means \pm SEM. **B.** Reporter cells were treated with 6N-Tet (2 μ M) and NR activity was tested. Data was normalized to receptor activity with an agonist concentration of EC₁₀₀.

DISCUSSION:

LRH-1 is a nuclear receptor that is known to bind PLs (Musille et al., 2012). While early small molecule agonists of LRH-1 bound deep within the pocket, mimicking binding patterns similar to phospholipids helps improve compound potency and efficacy (Flynn et al., 2018; Mays et al., 2016; Mays et al., 2022; Whitby et al., 2011). Here, we examined a new class of compounds that aimed at modifying pocket mouth interactions. Tet was the only isostere to have a similar affinity to that of 10CA. This small molecule also had increased potency in reporter assays and drove higher expression of target genes *NR0B2* and *CYP7A1* in HepG2 cells. The tetrazole also bound very similarly to 10CA within the LRH-1 LBD. The only notable difference was that the tetrazole didn't contact K520, which may be due to protonation at low pH in crystal conditions. MD simulations suggest that the tetrazole makes stronger contacts at the pocket mouth due to the tetrazole interacting with G421 for >60% of simulations, whereas 10CA only interacted with this residue for ~5% of simulations. Additionally, Tet interacted with K520 and Y516 for two times as long as 10CA.

The tetrazole is deprotonated due to its aromatic characteristic, giving a negative charge at the physiological pH, similar to the carboxylic acids, allowing for extensive hydrogen bonding and electrostatic engagement with K520. Additionally, the tetrazole consists of four atoms that can hydrogen bond versus the two in the carboxylic acid, which may account for the high potency, affinity, thermal stability, and stronger interactions seen in the MD simulations.

Tetrazole derivatives are a robust class that is well-defined within the realm of medicinal chemistry (Hansch and Leo, 1995; Herr, 2002; Juby and Hudyma, 1969; Myznikov et al., 2007). Recently, compounds containing tetrazoles have been used for a wide variety of novel drugs as antifungals, antibacterials, and antihypertensives (Zou et al., 2020). Carboxylic acids are not

always ideal due to their potential limited permeability across cell membranes and metabolic instability (Herbst and Wilson, 2002; Herr, 2002; Kaczmarek et al., 1979; Liljebris et al., 2002; Matta et al., 2010; McManus and Herbst, 2002; Neochoritis et al., 2019). Additionally, the hydrogen bonding environment of the tetrazole extends 1.2 Å farther than the carboxylic acid (Allen et al., 2012). Given this, a shorter linker length of nine carbons might be better suited for the tetrazole compound.

Tetrazoles are not a functional group commonly found within biological contexts, decreasing the potential degradation via metabolic pathways (Figdor and von ittenau, 1967; Herr, 2002; Holland and Pereira, 1967; Myznikov et al., 2007; Neochoritis et al., 2019). Tetrazoles have increased lipophilicity relative to that of carboxylic acids, which may account for the increased target gene expression within HepG2 cells (Hansch and Leo, 1995; Herr, 2002; Kraus, 1983).

Previously, studies have shown that the addition of a sulfamide in place of the hydroxyl on the RJW100 scaffold improves potency of the compound (Mays et al., 2019). Recently, it has also been shown that appending this sulfamide to the 10CA scaffold (6N-10CA) improves affinity and potency 30 times greater than that of 10CA (Cato et al., 2022). Due to the high binding affinity and high efficacy in reporter assays, we used a similar approach, synthesizing a small molecule with the Tet tail and sulfamide anchoring group (6N-Tet). 6N-Tet was able to maintain the efficacy of Tet and displayed increased affinity and potency. However, this small molecule displayed modestly improved affinity and potency over Tet (two-fold).

Cross-reactivity across various nuclear receptors is a concern due to the potentially vast physiological side effects, so we aimed to examine the specificity of our ligands. There was minimal reactivity with other nuclear receptors but high cross-reactivity with LRH-1's homolog

SF-1, which was expected due to their high similarity in the LBD (Meinsohn et al., 2019; Yazawa et al., 2015). However, further modifications to this group of LRH-1 agonists might provide a path to increase specificity towards LRH-1.

Overall, the tetrazole moiety is an effective way to contact pocket mouth residues of LRH-1. Tet shows improved potency, efficacy, and stronger hydrogen bonding with PL-binding residues at the mouth of the pocket. 6N-Tet also represents a selective NR5A agonist that maintains strong LRH-1 agonism. Ultimately, this small molecule can provide a new pathway to explore the effects of LRH-1 within pathophysiological contexts.

METHODS:

Chemical Synthesis.

Cell culture. Cells were cultured under standard conditions (5% CO₂, 37°C). HepG2 cells were cultured in phenol red-free DMEM + 10% fetal bovine serum (FBS). HeLa cells were cultured in phenol red-free MEM α + 10% FBS – charcoal/dextran treated (FBS-S).

Data analysis and visualization. Average values from technical replicates were used for all data analyses. These values represented either biological replicates (in-cell work) or independent experiments (*in vitro* work) that were combined for data analyses. Bar charts and curves were constructed with GraphPad Prism version 9, structural figures were constructed with either PyMol or VMD (Humphrey et al., 1996), and difference distance matrices were constructed with Bio3D (Grant et al., 2006). GraphPad Prism version 9 was used for all data analyses. All figures were constructed using Adobe Illustrator 2021 (Adobe Inc.). Values were consistently reported with two significant figures.

Protein purification. LRH-1 LBD was expressed and purified as described previously (Cato et al., 2022). Briefly, BL21(DE3) *E. coli* cells were transformed with human LRH-1 LBD (residues 299-541) with an N-terminal 6xHis tag in a pMCSG7 vector. Cells were grown at 37°C in liquid broth until OD₆₀₀ 0.6. Protein expression was induced with 1 mM IPTG for 4 hours at 30°C. Cells were centrifuged and stored at -80°C. The cell pellet was resuspended in lysis buffer (20 mM Tris-HCl, 150 mM NaCl, 5% glycerol, 25 mM imidazole, 0.2 mM phenylmethylsulfonyl fluoride, DNase, lysozyme, pH 7.4) and lysed via sonication. Protein was isolated with Ni²⁺ affinity chromatography. Human LRH-1 LBD purifies bound to bacterial phospholipids when expressed in *E. coli* (Ortlund et al., 2005). We removed co-purified bacterial lipids for LRH-1 LBD used in FP competition assays by incubating the protein with four-fold molar excess of

DLPC overnight at 4°C. LBD was then purified with size-exclusion chromatography (SEC) into assay buffer (150 mM NaCl, 20 mM Tris-HCl, 5 % glycerol, pH 7.4). LRH-1 LBD used for thermal stability assays was purified in a similar manner but was not complexed with DLPC prior to SEC purification. LRH-1 LBD used for crystallography was incubated with TEV protease to remove the 6xHis tag and subjected to a second round of Ni²⁺ affinity chromatography before being complexed with Tet (see below). All protein was stored at -80°C until use.

Fluorescence polarization competition assays. Forward binding assays were run as described previously (D'Agostino et al., 2020). Briefly, binding affinity for 6N conjugated to fluorescein amidite (FAM) was determined using 10 nM 6N-FAM and protein concentrations indicated in the figure (**Fig. S1**). Plates were incubated overnight at 4°C. Polarization was monitored on a Neo plate reader (Biotek, Winooski, VT) at an excitation/emission wavelength of 485/528 nm. Eight independent experiments were conducted, each with three technical replicates. Data were baseline-corrected and fit with a one-site binding (total) curve in GraphPad Prism version 9. The resulting curve is provided in supplemental information (**Fig. S1**) and the K_d was 8.1 nM.

FP competition assays were conducted as described previously (Cato et al., 2022; D'Agostino et al., 2020). Briefly, experiments were conducted in 30 µL of assay buffer (150 mM NaCl, 20 mM Tris-HCl, 5% glycerol, pH 7.4). 6N-FAM (10 nM/well) was incubated with LRH-1 LBD (5 nM/well). Unlabeled compounds were added at concentrations indicated in figures, with DMSO in each well held constant at 6.7% v/v. Data were excluded from analysis from wells with 1e-4 M Am and HA, as the corresponding polarization values distorted the curve fit because they were abnormally high potentially as a result of compound insolubility. Each experiment was performed two times with four technical replicates each. Technical replicates were averaged and

normalized independently prior to final data analysis. Using GraphPad Prism (version 9), data from each independent experiment were first normalized so that the highest and lowest values corresponded to 100 and zero, respectively. Data were then fit to a one-site, fit K_i curve, assuming a final probe concentration of 10 nM and probe affinity ($K_d = 8.1$ nM) determined with forward binding assays (**Fig. S1**).

Thermal stability assays. Thermal stability of the LRH-1 LBD complexed with ligands was determined as described previously (Cato et al., 2022) using a TychoTM NT.6 Nanotemper. LRH-1 LBD was incubated with 5-fold molar excess of ligand (final DMSO concentration was 1.4%) overnight at 4°C in assay buffer (150 mM NaCl, 20 mM Tris-HCl, 5% glycerol, pH 7.4). Complexes were centrifuged at high speed for five minutes and then loaded into capillaries. Tryptophan/tyrosine fluorescence was monitored at wavelengths 330 and 350 nm over a 30°C/min gradient (35°C – 95°C). The inflection point was determined with TychoTM NT.6 software. Two separate experiments were conducted with three technical replicates, which were averaged and plotted using GraphPad Prism (version 9).

Luciferase reporter assays. LRH-1 reporter assays were conducted as described previously (Cato et al., 2022; Mays et al., 2016). Briefly, HeLa cells were seeded at ~7,500 cells per well in 96-well plates (white-walled, clear bottom) in MEM α + 10% FBS-S. Once cells reached 70-90% confluence, they were transfected with LRH-1 (in pCI vector, 5 ng/well), a reporter plasmid with an NR5A response element derived from the SHP promoter cloned upstream of firefly luciferase (in pGL3-Basic vector, 50 ng/well), and a plasmid expressing Renilla luciferase constitutively from a CMV promoter (1 ng/well) (Mays et al., 2022). Cells were transfected with FuGENE at a ratio of 2.5:1 (FuGENE:DNA). Twenty-four hours after transfection, compounds were diluted in Opti-MEM and introduced to cells at final concentrations indicated in figures (final DMSO

concentration was 0.37%). Luciferase signal was measured after 24 hours using the DualGlo kit (Promega) with a Neo plate reader (Biotek, Winooski, VT). Experiments were conducted with three biological replicates, each with three technical replicates averaged prior to data analysis. Each well's Firefly luciferase signal intensity was divided by the well's Renilla signal intensity and then normalized relative to the DMSO control. Data were analyzed with GraphPad Prism (version 9) using a stimulating dose-response curve (Hill slope = 1). The fold change was determined to be the calculated span + 1. Relative efficacies reported were determined by dividing the small molecule's fold change by that of 10CA. Data were excluded from analysis for cells treated with 3×10^{-5} M of Tet and Sul as low Renilla signal and cell morphology suggested cytotoxicity. Data was included for this concentration in reporter assays comparing Tet and 6N-Tet, as there was no observable cell death during these experiments.

RT-qPCR. RT-qPCR was performed as described previously (Cato et al., 2022). HepG2 cells were seeded at 400,000 cells per well in 24-well plates in DMEM + 10% FBS. When cells reached ~ 90% confluence, media was exchanged with media containing DMSO or compound at the desired concentration (final DMSO concentration: 0.3%). Small molecules were added concentrations indicated in figure legends. After 24 hours, media was decanted, cells were washed with phosphate buffered saline, and cells were collected in RLT lysis buffer (+ 1% 2-mercaptoethanol). Cells were stored at -80°C prior to RNA extraction. RNA was extracted from cells using the RNeasy® Mini Kit (QIAGEN), with on-column DNase digestion. RNA was reverse transcribed with the High-Capacity cDNA Reverse Transcription Kit (Applied Biosystems™). cDNA was quantified using Power SYBR Green PCR Master Mix (Applied Biosystems™), using human *ACTB* (Actin Beta) as a housekeeping gene. Ct values were calculated by resident software on the StepOne Plus thermocycler. Data were normalized using

the $\Delta\Delta C_t$ method (Livak and Schmittgen, 2001). Each experiment was conducted with two or four biological replicates that were normalized independently for data analysis. Data were analyzed with GraphPad Prism, using a Brown-Forsythe and Welch One-Way ANOVA and Dunnett T3 Multiple Comparisons Test. Primers used for RT-qPCR were as follows:

hACTB (Chiang et al., 2019)

forward 5'-AGGCACCAGGGCGTGAT-3'

reverse 5'-GCCCACATAGGAATCCTTCTGAC-3'

hSHP (Whitby et al., 2011)

forward 5'-GCTTAGCCCCAAGGAATATGC-3'

reverse 5'-GTTCCAGGACTTCACACAGC-3'

hCYP7A1 (Bu et al., 2017)

forward 5'-GAGAAGGCAAACGGGTGAAC-3'

reverse 5'-GGATTGGCACCAAATTGCAGA-3'

X-ray crystallography. LRH-1 LBD-Tet crystals were generated as described previously (Cato et al., 2022; Cornelison et al., 2020; Mays et al., 2022). Briefly, cleaved (6xHis tag removed) LRH-1 LBD was incubated with Tet at four-fold molar excess overnight at 4°C. The complex was then purified via SEC into crystallization buffer (150 mM NaCl, 100 mM ammonium acetate, 1 mM EDTA, 2 mM CHAPS, 1 mM DTT, pH 7.4) and incubated with a peptide corresponding to human TIF2 NR box 3 (^+H_3N -KENALLRYLLDKDD- CO_2^-) at four-fold molar excess, along with an additional two-fold molar excess of Tet, for two hours at room temperature. The complex was then concentrated to ~ 7 mg/mL and crystals were generated via hanging drop vapor diffusion in crystallant containing 0.1 M tri-Na citrate – pH 4.6, 10-14% tert-butanol, and 0-7.5% glycerol at 4°C. Crystals were flash frozen in liquid N₂ using cryoprotectant

consisting of crystallant supplemented with 30% glycerol. Data were collected remotely from the Southeast Regional Collaborative Access Team (SER-CAT) at the Advanced Photon Source (Argonne National Laboratories, Chicago, IL). Data were processed using HKL2000 and phased with molecular replacement, using PDB 4DOS as the search model (Musille et al., 2012).

Structure refinement was performed with Phenix (Adams et al., 2010; Afonine et al., 2012) and Coot (Emsley et al., 2010). Additional refinement was performed with PDB-REDO (Joosten et al., 2014). Twinning was detected with xtriage in Phenix, and we used the recommended twin law (-h,-k,l) during refinement. Final figures were constructed with PyMOL (Schrödinger, LLC), which was also used to predict hydrogen bonds between the ligand and pocket mouth.

Model construction. Complexes for MD simulations with LRH-1 LBD were constructed as described previously (Cato et al., 2022). Three complexes were included: i) apo LRH-1-TIF2; ii) LRH-1-TIF2-Tet; and iii) LRH-1-TIF2-10CA. Ligand-bound (or apo) LRH-1 LBD complexes were generated by using the structure of LRH-1-TIF2-Tet (PDB 8F8M) as a starting model. Note that PDB 8F8M underwent further refinement before being uploaded to PDB but was nearly identical to that used for MD studies. 10CA was modeled into the complex using the positioning of the ligand from the previous crystal structure (PDB 7JYD). Complexes included LRH-1 residues 299-540 and residues 742-752 of TIF2 ($^+H_3N-NALLRYLLDKD-CO_2^-$). Residues 539 and 540 were added using the positioning from PDB 7JYE.

Maestro (Schrödinger, LLC) was used to optimize hydrogen bond assignments (pH 7.0), add N- and C-terminal caps to LRH-1 and TIF2, and run initial minimization on the structure. The complexes were solvated in an octahedral box of TIP3P water with a 10 Å buffer around the protein complex. Na^+ and Cl^- ions were added to neutralize the protein and achieve physiological buffer conditions (150 mM NaCl). Systems were set up using the xleap tool in AmberTools20 of

Amber 2020 (Case et al., 2020), with ff14SB (Maier et al., 2015) (protein), GAFF2 (Wang et al., 2004) (ligand), and TIP3P (Jorgensen et al., 1983) (water) forcefields. Parameters for 10CA and Tet were obtained using Antechamber (Wang et al., 2001) in AmberTools20. Note that both ligands were deprotonated in simulations, giving each a net charge of -1.

Molecular dynamics simulations. MD simulations were performed as described previously (Cato et al., 2022; Mays et al., 2019). For minimization, 5000 steps of steepest descent were used, followed by 5000 steps of conjugate gradient minimization. Minimizations were first performed with 500 kcal/mol·Å² restraints on all protein and ligand atoms. Restraints were then removed on all atoms except the ligand and TIF2 peptide, and the protocol was repeated. Restraints were then removed on all atoms except the ligand, and the protocol was repeated. Restraints were subsequently lowered to 100 kcal/mol·Å² and then finally removed from all atoms for two final rounds of minimization. Minimized systems were heated from 0 to 300 K with a 100-ps MD run, with constant volume periodic boundaries and 10 kcal/mol·Å² restraints on all protein and ligand atoms. A 10-ns equilibration was performed for all complexes with 10 kcal/mol·Å² restraints on all protein and ligand atoms using the NPT ensemble. Restraints were then removed on all atoms except the ligand, and the protocol was repeated. The protocol was repeated with a 1 kcal/mol·Å² restraint on the ligand. Note that the water molecules critical for ligand engagement deep within the pocket (four waters) and at the mouth (one water) were restrained along with ligand.

Production trajectories of 500-ns were obtained for unrestrained complexes in the NPT ensemble. All bonds between heavy atoms and hydrogens were fixed with the SHAKE algorithm (Ryckaert et al., 1977). A cutoff distance of 10 Å was used to evaluate long-range electrostatics with particle mesh Ewald and for van der Waals forces. Structural averaging was performed

using the CPPTRAJ (Roe and Cheatham, 2013) module of AmberTools. Four 500-ns simulations were run and concatenated with CPPTRAJ (Roe and Cheatham, 2013), with every fifth frame (total of 40,000 frames) used for data analysis. Water, Na⁺, Cl⁻, along with N- and C-terminal caps, were removed for data analysis.

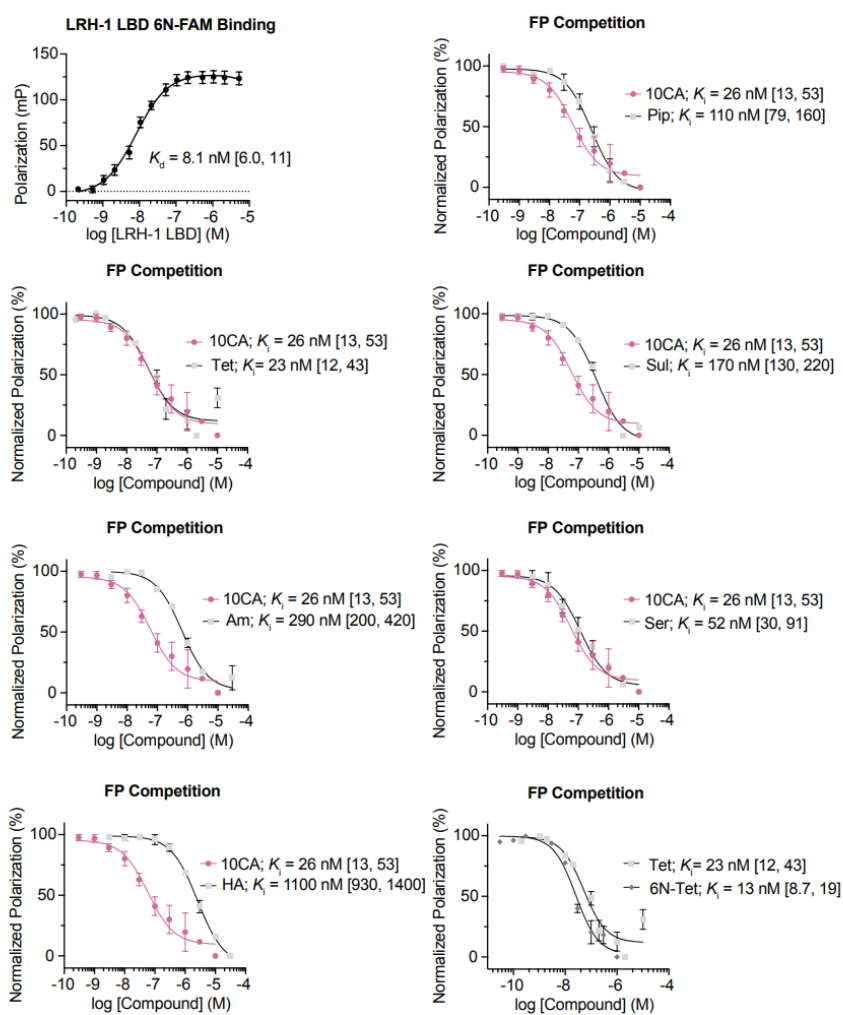
CPPTRAJ (Roe and Cheatham, 2013) was used to for hydrogen bond analyses, as well as the construction of average structures. Note that hydrogen bond analysis was conducted with the default angle cutoff of 135° and distance cutoff of 3.5 Å. Bio3D (Grant et al., 2006) was used to create difference distance matrices comparing average structures between apo and ligand-bound complexes. Dynamic networks were constructed from trajectories using the NetworkView plugin (Sethi et al., 2009) in VMD (Humphrey et al., 1996) and the Carma program (Glykos, 2006).

Networks were constructed by defining all protein C α atoms as nodes, using Cartesian covariance (calculated in Carma) to measure communication within the network. Hydrogen atoms were excluded from network construction, and edges between neighboring residues were disallowed. Pairs of nodes that reside within a 4.5 Å cutoff for 75% of the simulation are connected via an edge. Communities are constructed using the Girvan-Newman algorithm, and the minimum number of communities possible were generated while maintaining at least 98% maximum modularity (Girvan and Newman, 2002; Newman, 2006). Communities were visualized with VMD (Humphrey et al., 1996).

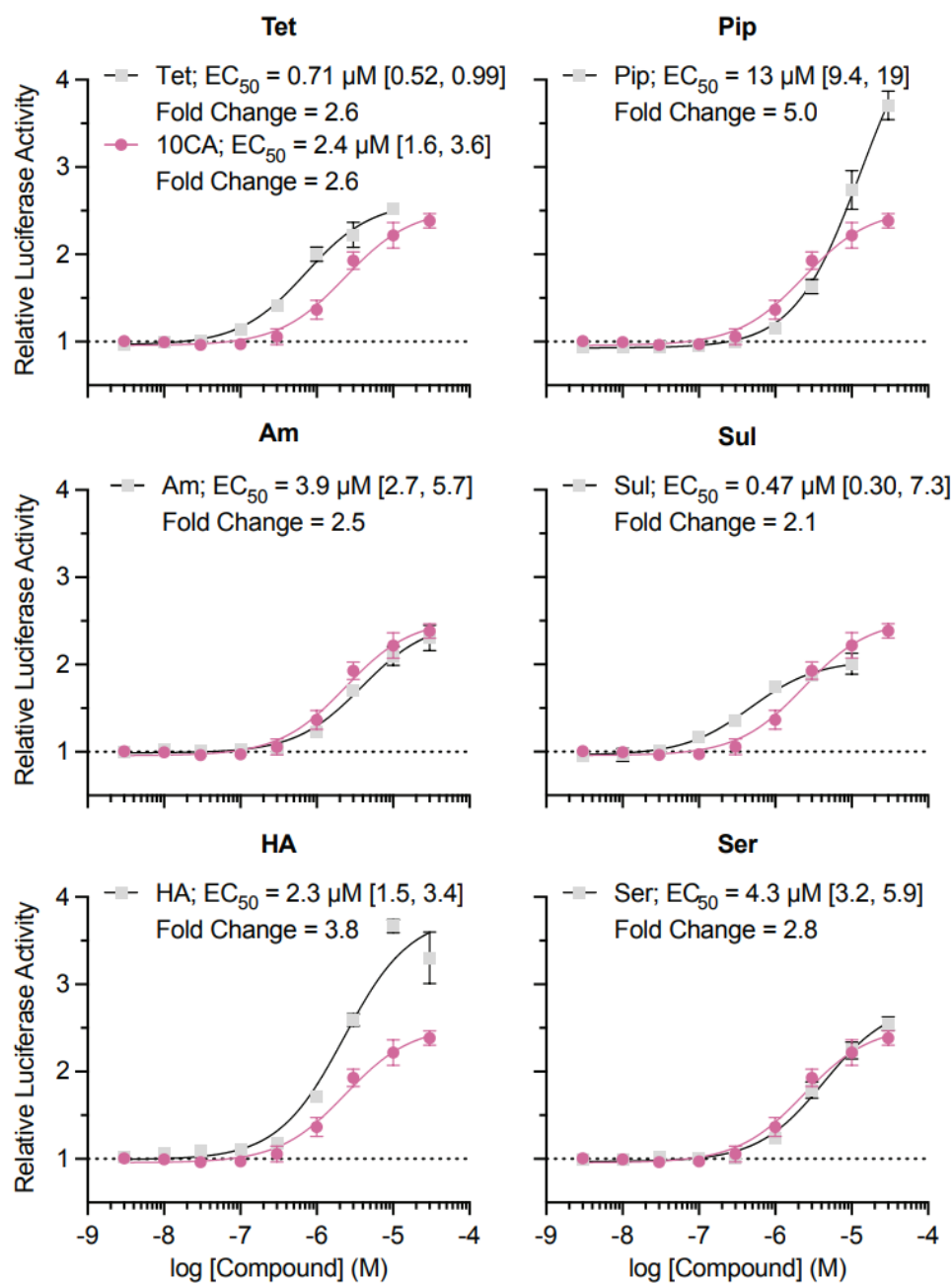
Cross-reactivity studies. Reporter assays comparing LRH-1 and SF-1 activity were conducted as above. However, for experiments testing SF-1 activity, cells were transfected with SF-1 in a pcDNA vector (5 ng/well). Cells were transfected with FuGENE at a ratio of 4:1 (FuGENE:DNA). Cells were treated with 10 μ M of compound for 24 hours (final DMSO concentration was 0.37%). Reporter assays assessing cross-reactivity with non-NR5A receptors

were conducted by INDIGO Biosciences, Inc. Reporter cells expressed either the native receptor (AhR, AR, ER α , GR, and MR) or a receptor hybrid in which the native N-terminal DBD has been replaced with that of the yeast Gal4 DBD (ROR γ , CAR3, FXR, PPAR α , PPAR δ , PPAR γ , and PXR). Huh7 (AhR), CV-1 (AR), CHO (CAR3, ER α , FXR, GR, PPAR α , PPAR δ , and PPAR γ), or HEK293 (ROR γ , MR, and PXR) cells were used in studies. A gene encoding Firefly luciferase was downstream of a receptor-specific genetic response element or the Gal4 upstream activation sequence. All reference compounds used, aside from ursolic acid (ROR γ inverse agonists), were agonists and were as follows: ursolic acid (ROR γ), MeBio (AhR), 5 α -Dihydro-11- ketoTestosterone (AR), CITCO (CAR3), 17 β -estradiol (ER α), GW4064 (FXR), dexamethasone (GR), aldosterone (MR), GW7647 (PPAR α), GW0742 (PPAR δ), rosiglitazone (PPAR γ), and rifampicin (PXR). Experiments were run in triplicate in 96-well plates (medium = cell recovery medium). Assay plates were incubated for 24 hours and then the treatment media was discarded. Luciferase Detection Reagent was added and relative bioluminescence was measured. All graphical manipulations were performed using GraphPad Prism software.

SUPPLEMENTAL INFORMATION:



Supplemental Figure 1. FP Binding and Competition for each isostere. Determination of the 6N-FAM binding affinity to LRH-1 LBD from the top left curve using FP binding. Data used from 8 independent experiments shown as mean \pm SEM, brackets have 95% confidence intervals. K_d = dissociation constant. FP competition was used to determine K_i (inhibition constant). Data shown as mean \pm SEM from two independent experiments, brackets have 95% confidence intervals. Polarization was normalized to a scale of the lowest value = 0, highest = 100. These K_i were used in Figure 3A and 6C



Supplemental Figure 2. Luciferase Reporter Assays. Effect of small molecules on LRH-1 activity determined through luciferase reporter activity. Data from three biological replicates normalized to DMSO control shown as mean \pm SEM, with brackets having the 95% confidence interval. Relative luciferase activity is corresponded to the calculated span of the curve + 1. EC₅₀ = half maximal effective concentration. Relative activity was normalized to that of 10CA and used to construct Figure 3C.

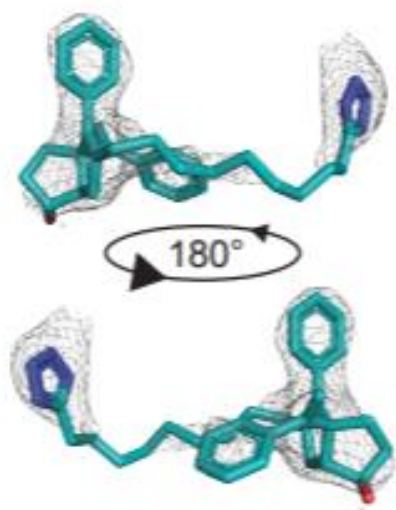


Figure S3. Tet omit map. Omit map for Fc – Fo contoured at 2.5σ

Data collection	LRH-1 + Tet + Tif2
Space group	P3 ₂ 21
Cell dimensions	
<i>a</i> , <i>b</i> , <i>c</i> (Å)	89.2, 89.2, 105.7
α , β , γ (°)	90, 90, 120
Resolution (Å)	44.6 - 2.60 (2.69 - 2.60)
Average <i>I</i> / σ	12.1 (1.38)
Completeness (%)	97.7 (81.7)
CC1/2	0.937 (0.570)
Redundancy	11.2
Unique reflections	15066 (1235)
Refinement	
R-work/R-free (%)	20.1/22.4
No. atoms	
Protein	2041
Ligand	37
Water	29
B-factors	
Protein	68.1
Ligand	58.5
Water	62.7
R.M.S. deviations	
Bond lengths (Å)	0.002
Bond angles (°)	0.49
Ramachandran favored (%)	96.4
Ramachandran outliers (%)	0.00
Twin law	-h,-k,l
PDB accession code	8F8M

Table S1: Data from X-ray crystallography.

REFERENCES

- Maestro, Schrödinger, LLC, New York, NY, 2021.
- The PyMOL Molecular Graphics System, Version 2.0 Schrödinger, LLC.
- Adams PD, Afonine PV, Bunkoczi G, Chen VB, Davis IW, Echols N, Headd JJ, Hung LW, Kapral GJ, Grosse-Kunstleve RW, McCoy AJ, Moriarty NW, Oeffner R, Read RJ, Richardson DC, Richardson JS, Terwilliger TC and Zwart PH (2010) PHENIX: a comprehensive Python-based system for macromolecular structure solution. *Acta Crystallogr D Biol Crystallogr* **66**(Pt 2): 213-221.
- Afonine PV, Grosse-Kunstleve RW, Echols N, Headd JJ, Moriarty NW, Mustyakimov M, Terwilliger TC, Urzhumtsev A, Zwart PH and Adams PD (2012) Towards automated crystallographic structure refinement with phenix.refine. *Acta Crystallogr D Biol Crystallogr* **68**(Pt 4): 352-367.
- Al-Bawardy B, Shivashankar R and Proctor DD (2021) Novel and Emerging Therapies for Inflammatory Bowel Disease. *Front. Pharmacol.* 12:651415
- Allen FH, Groom CR, Liebeschutz JW, Bardwell DA, Olsson TS and Wood PA (2012) The hydrogen bond environments of 1H-tetrazole and tetrazolate rings: the structural basis for tetrazole-carboxylic acid bioisosterism. *J Chem Inf Model* **52**(3): 857-866.
- Bayrer, J.R., Wang, H., Nattiv, R. *et al.* LRH-1 mitigates intestinal inflammatory disease by maintaining epithelial homeostasis and cell survival. *Nat Commun* **9**, 4055 (2018)
- Botrugno OA, Fayard E, Annicotte JS, Haby C, Brennan T, Wendling O, Tanaka T, Kodama T, Thomas W, Auwerx J and Schoonjans K (2004) Synergy between LRH-1 and beta-catenin induces G1 cyclin-mediated cell proliferation. *Mol Cell* **15**(4): 499-509.
- Bruscoli S, Febo M, Riccardi C, Migliorati G. Glucocorticoid Therapy in Inflammatory Bowel Disease: Mechanisms and Clinical Practice. *Front Immunol.* 2021 Jun 3;12:691480
- Bu P, Le Y, Zhang Y, Zhang Y and Cheng X (2017) Berberine-induced Inactivation of Signal Transducer and Activator of Transcription 5 Signaling Promotes Male-specific Expression of a Bile Acid Uptake Transporter. *J Biol Chem* **292**(11): 4602-4613.
- Case DA, Belfon K, Ben-Shalom IY, Brozell SR, Cerutti DS, Cheatham TEI, Cruzeiro VWD, Darden TA, Duke RE, Giambasu G, Gilson MK, Gohlke H, Goetz AW, Harris R, Izadi S, Izmailov SA, Kasavajhala K, Kovalenko A, Krasny R, Kurtzman T, Lee TS, LeGrand S, Li P, Lin C, Liu J, Luchko T, Luo R, Man V, Merz KM, Miao Y, Mikhailovskii O, Monard G, Nguyen H, Onufriev A, Pan F, Pantano S, Qi R, Roe DR, Roitberg A, Sagui C, Schott-Verdugo S, Shen J, Simmerling CL, Skrynnikov NR, Smith J, Swails J, Walker RC, Wang J, Wilson L, Wolf RM, Wu X, Xiong Y, Xue Y, York PA and Kollman DM (2020) AMBER 2020, University of California, San Francisco.
- Cato ML, Cornelison JL, Spurlin RM, Courouble VV, Patel AB, Flynn AR, Johnson AM, Okafor CD, Frank F, D'Agostino EH, Griffin PR, Jui NT and Ortlund EA (2022) Differential Modulation of Nuclear Receptor LRH-1 through Targeting Buried and Surface Regions of the Binding Pocket. *J Med Chem* **65**(9): 6888-6902.
- Chiang HC, Zhang X, Li J, Zhao X, Chen J, Wang HT, Jatoi I, Brenner A, Hu Y and Li R (2019) BRCA1-associated R-loop affects transcription and differentiation in breast luminal epithelial cells. *Nucleic Acids Res* **47**(10): 5086-5099.
- Choi S, Dong B, Lin CJ, Heo MJ, Kim KH, Sun Z, Wagner M, Putluri N, Suh JM, Wang MC and Moore DD (2020) Methyl-Sensing Nuclear Receptor Liver Receptor Homolog-1 Regulates Mitochondrial Function in Mouse Hepatocytes. *Hepatology* **71**(3): 1055-1069.
- Cornelison JL, Cato ML, Johnson AM, D'Agostino EH, Melchers D, Patel AB, Mays SG, Houtman R, Ortlund EA and Jui NT (2020) Development of a new class of liver receptor

- homolog-1 (LRH-1) agonists by photoredox conjugate addition. *Bioorg Med Chem Lett* **30**(16): 127293.
- Coste A, Dubuquoy L, Barnouin R, Annicotte JS, Magnier B, Notti M, Corazza N, Antal MC, Metzger D, Desreumaux P, Brunner T, Auwerx J and Schoonjans K (2007) LRH-1-mediated glucocorticoid synthesis in enterocytes protects against inflammatory bowel disease. *Proc Natl Acad Sci U S A* **104**(32): 13098-13103.
- D'Agostino EH, Flynn AR, Cornelison JL, Mays SG, Patel A, Jui NT and Ortlund EA (2020) Development of a Versatile and Sensitive Direct Ligand Binding Assay for Human NR5A Nuclear Receptors. *ACS Med Chem Lett* **11**(3): 365-370.
- Emsley P, Lohkamp B, Scott WG and Cowtan K (2010) Features and development of Coot. *Acta Crystallogr D Biol Crystallogr* **66**(Pt 4): 486-501.
- Evans RM and Mangelsdorf DJ (2014) Nuclear Receptors, RXR, and the Big Bang. *Cell* **157**(1): 255-266.
- Fernandez-Marcos PJ, Auwerx J and Schoonjans K (2011) Emerging actions of the nuclear receptor LRH-1 in the gut. *Biochim Biophys Acta* **1812**(8): 947-955.
- Figdor SK and von ittenau MS (1967) Metabolism of 5-(3-pyridyl)tetrazole. *J Med Chem* **10**(6): 1158-1159.
- Flynn AR, Mays SG, Ortlund EA and Jui NT (2018) Development of Hybrid Phospholipid Mimics as Effective Agonists for Liver Receptor Homologue-1. *ACS Med Chem Lett* **9**(10): 1051-1056.
- Friedman HL (1951) Influence of Isosteric Replacements upon Biological Activity, p 295–358, NAS-NRS, Washington, DC.
- Girvan M and Newman MEJ (2002) Community structure in social and biological networks. *Proceedings of the National Academy of Sciences* **99**: 7821-7826.
- Glykos NM (2006) Software news and updates. Carma: a molecular dynamics analysis program. *J Comput Chem* **27**(14): 1765-1768.
- Grant BJ, Rodrigues AP, ElSawy KM, McCammon JA and Caves LS (2006) Bio3d: an R package for the comparative analysis of protein structures. *Bioinformatics* **22**(21): 2695-2696.
- Hansch C and Leo A (1995) Exploring QSAR: Fundamentals and Applications in Chemistry and Biology, American Chemical Society, Washington DC.
- Herbst RM and Wilson KR (2002) Apparent Acidic Dissociation of Some 5-Aryltetrazoles. *The Journal of Organic Chemistry* **22**(10): 1142-1145.
- Herr RJ (2002) 5-Substituted-1H-tetrazoles as carboxylic acid isosteres: medicinal chemistry and synthetic methods. *Bioorg Med Chem* **10**(11): 3379-3393.
- Holland GF and Pereira JN (1967) Heterocyclic tetrazoles, a new class of lipolysis inhibitors. *J Med Chem* **10**(2): 149-154.
- Humphrey W, Dalke A and Schulten K (1996) VMD: visual molecular dynamics. *J Mol Graph* **14**(1): 33-38, 27-38.
- Joosten RP, Long F, Murshudov GN and Perrakis A (2014) The PDB_REDO server for macromolecular structure model optimization. *IUCrJ* **1**(Pt 4): 213-220.
- Jorgensen WL, Chandrasekhar J, Madura JD, Impey RW and Klein ML (1983) Comparison of simple potential functions for simulating liquid water. *The Journal of Chemical Physics* **79**(2): 926-935.

- Juby PF and Hudyma TW (1969) Preparation and antiinflammatory properties of some 1-substituted 3-(5-tetrazolylmethyl)indoles and homologs. *J Med Chem* **12**(3): 396-401.
- Kaczmarek Jz, Smagowski H and Grzonka Z (1979) A correlation of substituent effects with the acidity of aromatic tetrazolic acids. *Journal of the Chemical Society, Perkin Transactions* **2**(12).
- Kraus JL (1983) Isosterism and molecular modification in drug design: tetrazole analogue of GABA: effects on enzymes of the gamma-aminobutyrate system. *Pharmacol Res Commun* **15**(2): 183-189.
- Lassalas P, Gay B, Lasfargeas C, James MJ, Tran V, Vijayendran KG, Brunden KR, Kozlowski MC, Thomas CJ, Smith AB, 3rd, Huryn DM and Ballatore C (2016) Structure Property Relationships of Carboxylic Acid Isosteres. *J Med Chem* **59**(7): 3183-3203.
- Lee JM, Lee YK, Mamrosh JL, Busby SA, Griffin PR, Pathak MC, Ortlund EA and Moore DD (2011) A nuclear-receptor-dependent phosphatidylcholine pathway with antidiabetic effects. *Nature* **474**(7352): 506-510.
- Li Y, Lambert MH and Xu HE (2003) Activation of nuclear receptors: a perspective from structural genomics. *Structure* **11**(7): 741-746.
- Liljebris C, Larsen SD, Ogg D, Palazuk BJ and Bleasdale JE (2002) Investigation of potential bioisosteric replacements for the carboxyl groups of peptidomimetic inhibitors of protein tyrosine phosphatase 1B: identification of a tetrazole-containing inhibitor with cellular activity. *J Med Chem* **45**(9): 1785-1798.
- Livak KJ and Schmittgen TD (2001) Analysis of relative gene expression data using real-time quantitative PCR and the 2(-Delta Delta C(T)) Method. *Methods* **25**(4): 402-408.
- Lonard DM and O'Malley B W (2007) Nuclear receptor coregulators: judges, juries, and executioners of cellular regulation. *Mol Cell* **27**(5): 691-700.
- Maier JA, Martinez C, Kasavajhala K, Wickstrom L, Hauser KE and Simmerling C (2015) ff14SB: Improving the Accuracy of Protein Side Chain and Backbone Parameters from ff99SB. *J Chem Theory Comput* **11**(8): 3696-3713.
- Matta CF, Arabi AA and Weaver DF (2010) The bioisosteric similarity of the tetrazole and carboxylate anions: clues from the topologies of the electrostatic potential and of the electron density. *Eur J Med Chem* **45**(5): 1868-1872.
- Mays SG, D'Agostino EH, Flynn AR, Huang X, Wang G, Liu X, Millings EJ, Okafor CD, Patel A, Cato ML, Cornelison JL, Melchers D, Houtman R, Moore DD, Calvert JW, Jui NT and Ortlund EA (2022) A phospholipid mimetic targeting LRH-1 ameliorates colitis. *Cell Chem Biol* **29**(7): 1174-1186 e1177.
- Mays SG, Flynn AR, Cornelison JL, Okafor CD, Wang H, Wang G, Huang X, Donaldson HN, Millings EJ, Polavarapu R, Moore DD, Calvert JW, Jui NT and Ortlund EA (2019) Development of the First Low Nanomolar Liver Receptor Homolog-1 Agonist through Structure-guided Design. *J Med Chem* **62**(24): 11022-11034.
- Mays SG, Okafor CD, Whitby RJ, Goswami D, Stec J, Flynn AR, Dugan MC, Jui NT, Griffin PR and Ortlund EA (2016) Crystal Structures of the Nuclear Receptor, Liver Receptor Homolog 1, Bound to Synthetic Agonists. *J Biol Chem* **291**(49): 25281-25291.
- McKenna NJ, Lanz RB and O'Malley BW (1999) Nuclear receptor coregulators: cellular and molecular biology. *Endocr Rev* **20**(3): 321-344.
- McManus JM and Herbst RM (2002) Tetrazole Analogs of Amino Acids1. *The Journal of Organic Chemistry* **24**(11): 1643-1649.

- Meinsohn MC, Smith OE, Bertolin K and Murphy BD (2019) The Orphan Nuclear Receptors Steroidogenic Factor-1 and Liver Receptor Homolog-1: Structure, Regulation, and Essential Roles in Mammalian Reproduction. *Physiol Rev* **99**(2): 1249-1279.
- Mueller M, Cima I, Noti M, Fuhrer A, Jakob S, Dubuquoy L, Schoonjans K and Brunner T (2006) The nuclear receptor LRH-1 critically regulates extra-adrenal glucocorticoid synthesis in the intestine. *J Exp Med* **203**(9): 2057-2062.
- Musille PM, Kossmann BR, Kohn JA, Ivanov I and Ortlund EA (2016) Unexpected Allosteric Network Contributes to LRH-1 Co-regulator Selectivity. *J Biol Chem* **291**(3): 1411-1426.
- Musille PM, Pathak M, Lauer JL, Hudson WH, Griffin PR and Ortlund EA (2012) Antidiabetic phospholipid-nuclear receptor complex reveals the mechanism for phospholipid-driven gene regulation. *Nat Struct Mol Biol* **19**(5): 532-S532.
- Myznikov LV, Hrabalek A and Koldobskii GI (2007) Drugs in the tetrazole series. (Review). *Chemistry of Heterocyclic Compounds* **43**(1): 1-9.
- Nagy L and Schwabe JW (2004) Mechanism of the nuclear receptor molecular switch. *Trends Biochem Sci* **29**(6): 317-324.
- Neochoritis CG, Zhao T and Domling A (2019) Tetrazoles via Multicomponent Reactions. *Chem Rev* **119**(3): 1970-2042.
- Newman ME (2006) Modularity and community structure in networks. *Proc Natl Acad Sci U S A* **103**(23): 8577-8582.
- Ortlund EA, Lee Y, Solomon IH, Hager JM, Safi R, Choi Y, Guan Z, Tripathy A, Raetz CR, McDonnell DP, Moore DD and Redinbo MR (2005) Modulation of human nuclear receptor LRH-1 activity by phospholipids and SHP. *Nat Struct Mol Biol* **12**(4): 357-363.
- Roe DR and Cheatham TE, 3rd (2013) PTRAJ and CPPTRAJ: Software for Processing and Analysis of Molecular Dynamics Trajectory Data. *J Chem Theory Comput* **9**(7): 3084-3095.
- Ryckaert J-P, Ciccotti G and Berendsen HJC (1977) Numerical integration of the cartesian equations of motion of a system with constraints: molecular dynamics of n-alkanes. *Journal of Computational Physics* **23**(3): 327-341.
- Elena P. Sablin, Irina N. Krylova, Robert J. Fletterick, Holly A. Ingraham (2003) Structural Basis for Ligand-Independent Activation of the Orphan Nuclear Receptor LRH-1. *Molecular Cell*, Volume 11, Issue 6, 2003: Pages 1575-1585,
- Sablin EP, Krylova IN, Fletterick RJ, Ingraham HA. Structural basis for ligand-independent activation of the orphan nuclear receptor LRH-1. *Mol Cell*. 2003 Jun;11(6):1575-85.
- Sethi A, Eargle J, Black AA and Luthey-Schulten Z (2009) Dynamical networks in tRNA:protein complexes. *Proc Natl Acad Sci U S A* **106**(16): 6620-6625.
- Stein S and Schoonjans K (2015) Molecular basis for the regulation of the nuclear receptor LRH-1. *Curr Opin Cell Biol* **33**: 26-34.
- Song, X., Kaimal, R., Yan, B., & Deng, R. (2008). Liver receptor homolog 1 transcriptionally regulates human bile salt export pump expression. *Journal of Lipid Research*, *49*(5), 973-984.
- Vanwart AT, Eargle J, Luthey-Schulten Z and Amaro RE (2012) Exploring residue component contributions to dynamical network models of allostery. *J Chem Theory Comput* **8**(8): 2949-2961.

- Wang J, Wolf RM, Caldwell JW, Kollman PA and Case DA (2004) Development and testing of a general amber force field. *J Comput Chem* **25**(9): 1157-1174.
- Wang JM, Wang W and Kollman PA (2001) Antechamber: An accessory software package for molecular mechanical calculations. *Abstracts of Papers of the American Chemical Society* **222**: U403-U403.
- Wassermann AM and Bajorath J (2011) Identification of target family directed bioisosteric replacements. *MedChemComm* **2**(7): 601-606.
- Weikum ER, Liu X and Ortlund EA (2018) The nuclear receptor superfamily: A structural perspective. *Protein Sci* **27**(11): 1876-1892.
- Whitby RJ, Dixon S, Maloney PR, Delerive P, Goodwin BJ, Parks DJ and Willson TM (2006) Identification of small molecule agonists of the orphan nuclear receptors liver receptor homolog-1 and steroidogenic factor-1. *J Med Chem* **49**(23): 6652-6655.
- Whitby RJ, Stec J, Blind RD, Dixon S, Leesnitzer LM, Orband-Miller LA, Williams SP, Willson TM, Xu R, Zuercher WJ, Cai F and Ingraham HA (2011) Small molecule agonists of the orphan nuclear receptors steroidogenic factor-1 (SF-1, NR5A1) and liver receptor homologue-1 (LRH-1, NR5A2). *J Med Chem* **54**(7): 2266-2281.
- Xiao L, Wang Y, Liang W, Liu L, Pan N, Deng H, Li L, Zou C, Chan FL and Zhou Y (2018) LRH-1 drives hepatocellular carcinoma partially through induction of c-myc and cyclin E1, and suppression of p21. *Cancer Manag Res* **10**: 2389-2400.
- Yazawa T, Imamichi Y, Miyamoto K, Khan MR, Uwada J, Umezawa A and Taniguchi T (2015) Regulation of Steroidogenesis, Development, and Cell Differentiation by Steroidogenic Factor-1 and Liver Receptor Homolog-1. *Zoolog Sci* **32**(4): 323-330.
- Xu F, Dahlhamer JM, Zammitti EP, Wheaton AG, Croft JB. Health-Risk Behaviors and Chronic Conditions Among Adults with Inflammatory Bowel Disease — United States, 2015 and 2016. *MMWR Morb Mortal Wkly Rep* 2018;67:190–195.
- Zou, Y., Liu, L., Liu, J., & Liu, G. (2020). Bioisosteres in drug discovery: Focus on tetrazole. *Future Medicinal Chemistry*, 12(2), 91-93.